JOURNAL OF APPLIED POLYMER SCIENCE VOL. 18, PP. 2569–2588 (1974)

An Experimental Study of Threadline Dynamics with Emphasis on the Effect of Molecular Weight on the Elongational Viscosity of Melt-Spun Poly(ethylene Terephthalate)

JACK W. HILL and JOHN A. CUCULO, *Department of Textile Chemistry, North Carolina State University, Raleigh, North Carolina 27607*

Synopsis

A study of a melt-spun threadline has been carried out to determine the effect of molecular weight on the elongational viscosity of the polymer being spun. Polymer chosen for this study was poly(ethylene terephthalate) having different molecular weights. Conventional nonisothermal spinning of the polymers was carried out with cooling by free convection. Threadline surface temperatures were measured by a null-balance technique. Threadline tension at the take-up device was measured, and samples of the threadline were taken to obtain linear density profiles. Nonlinear least-squares fits were applied to the linear density data to obtain equations for velocity and elongation rate. These measurements were then used to determine the threadline elongational viscosity. Least-squares fits were made to a polynomial relating absolute temperature and elongation rate to the elongational viscosity. These results were then used to determine an activation energy of elongational flow which was found to decrease with elongation rate. Elongational viscosity was found to increase with molecular weight.

INTRODUCTION

A thorough understanding of the dynamics of the melt-spun threadline is of fundamental importance. The phenomena occurring in the melt spinning process are intimately related to the properties of the finished fiber. Both experimental and theoretical studies of the melt spinning process have appeared in the literature.[1–7] There have also appeared in the literature several studies involving elongational viscosity, in not only the melt spinning process but also in the dry and wet spinning processes.[8–20] The ability of a material under stress to deform to some finite dimension, such as the final diameter in the spinning process, has been attributed to the occurrence of an increase in the elongational viscosity of the material. A study of elongational viscosity of polymeric materials is thus of considerable interest and importance.

Trouton[21] first introduced the concept of elongational viscosity in 1906 in a study of pitch, tar, and similar substances descending under their own weight. Trouton's studies were carried out isothermally, and no phase

change occurred. In his study, the force applied to these materials was solely that of gravity and very low elongation rates were observed. He found that the ratio of the axial tensile stress σ_{xx} to the elongation rate $\dot{\gamma}_E$ was a constant for the material, i.e., the elongational viscosity η_E or, as he termed it, "the coefficient of viscous traction." (The presence of viscoelastic effects in these materials imply that the quantity termed here as "elongational viscosity" is different from any kind of viscosity in the classical sense. This quantity has also been referred to by several authors as "tensile viscosity," "spinning viscosity," "consistency," "uniaxial extensional viscosity," etc.) Trouton's relation is given by

$$\eta_E = \frac{\sigma_{xx}}{\dot{\gamma}_E}. \tag{1}$$

It should be pointed out here that the elongation rate in elongational flow differs from the shear rate in shear flow. The elongation rate is in a direction parallel to the velocity, whereas in shear flow, the shear rate is in a direction perpendicular to the velocity.

Nitschmann and Schrade,[22] in 1948, and Ziabicki et al.,[1-3] at a later time, applied Trouton's formulations to the spinning process. Ziabicki,[3] in the melt spinning process, found the elongational viscosity of the spinning threadline to increase monotonically with distance from the spinnerette. Kase and Matsuo[4,5] in 1965, studied the elongational viscosity of a threadline of polypropylene and a threadline of a copolymer of poly(ethylene terephthalate) and poly(ethylene isophthalate). They, however, assumed elongational viscosity to be dependent only on temperature. In 1970, Ishibashi, Aoki, and Ishii,[14] in a study of nylon 6, also assumed that elongational viscosity depended only on temperature. In studying a range of number-average molecular weights $\bar{M}_n$ of 1.85×10^4 to 2.40×10^4, they concluded that within this molecular weight range the elongational viscosity was still dependent only on temperature. They point out, however, that in an unpublished study of a much wider range of $\bar{M}_n$, an increase in $\bar{M}_n$ did increase the elongational viscosity.

The studies cited thus far have failed to consider the importance of elongation rate in their study of elongational viscosity. In attempts to investigate the elongation rate effect, several workers, as pointed out by Lamonte and Han,[19] have carried out isothermal spinning studies. Considering the results of these studies, Lamonte and Han have proposed a generalized empirical equation which takes into account the dependence of elongational viscosity on both the elongation rate and the temperature of the threadline. These authors claim good agreement between the proposed equation and their own results on isothermal spinning studies of polystyrene, polyethylene, and polypropylene.

By making use of eq. (1) and the continuity equation expressed as

$$G = \rho A V = \text{constant} \tag{2}$$

where G is mass throughput rate, ρ is filament density, A is filament cross-sectional area, and V is the local velocity of the filament, it is possible to derive a more convenient form of eq. (1). Since G is a constant,

$$\frac{dG}{dx} = V\frac{d(\rho A)}{dx} + \rho A\frac{dV}{dx} = 0. \tag{3}$$

Solving eq. (3) for dV/dx yields

$$\dot{\gamma}_E = \frac{dV}{dx} = \frac{-V}{\rho A}\frac{d(\rho A)}{dx}. \tag{4}$$

And since the axial stress is given by

$$\sigma_{xx} = \frac{F_{\text{rheo}}}{A} \tag{5}$$

eq. (2) can be solved for A, and this can be substituted into eq. (5) to give

$$\sigma_{xx} = \frac{F_{\text{rheo}}\rho V}{G}. \tag{6}$$

Finally, substituting eqs. (4) and (6) into eq. (1) gives

$$\eta_E = -\frac{F_{\text{rheo}}\rho}{G}\left[\frac{1}{\rho A}\frac{d(\rho A)}{dx}\right]^{-1}. \tag{7}$$

This expression is used for determination of elongational viscosity in this study and was used in a similar form by Kase and Matsuo.[4,5] Using eq. (7), data for the threadline rheological force, density, mass throughput rate, and linear density are required for determining elongational viscosity.

In the present study, results are presented of our experimental investigations into the elongational flow behavior of threadlines of polyesters of various molecular weights. In all cases, nonisothermal studies were made. Threadline surface temperature data are used in conjunction with the elongational viscosity data to relate elongational viscosity and threadline temperature.

EXPERIMENTAL

Materials

The polymer chosen for this study was poly(ethylene terephthalate) of different molecular weights. The molecular weight characteristics of these polymers are given on Table I. Intrinsic viscosity (IV) was determined in 100% trifluoroacetic acid (0.4 g/dl) at 30°C, and the weight-average molecular weight ($\bar{M}_w$) was calculated from the relation given by Wallach.[23]

From Table I it is evident that the range of the molecular weight series has been reduced by the extrusion process. For this reason, experiments involving only polymers A, B, C, and D are discussed here.

TABLE I
Molecular Weight Characteristics of Polymer Chips and Filaments

Polymer	Chip		Filament	
	IV, dl/g	$\bar{M}_w \times 10^{-4}$	IV, dl/g	$\bar{M}_w \times 10^{-4}$
A	0.62	4.38	0.62	4.38
B[a]	0.69	5.12	0.65	4.69
C	0.76	5.90	0.71	5.34
D	0.82	6.60	0.79	6.25
E	0.85	6.96	0.80	6.37
F	0.88	7.32	0.80	6.37
G	0.92	7.82	0.78	6.13

[a] Contains 0.25% TiO_2

Apparatus and Procedures

All fiber spinning was carried out on a screw extruder manufactured by Reifenhauser of Germany. The extruder consists principally of an 18-mm screw and a 1.2-cm^3/rev gear metering pump. The screw delivers the molten polymer to the independently driven pump. The pump then delivers the material to a pack assembly of condensers and screens and finally to the spinnerette. A seven-hole spinnerette with 0.31-mm-diameter holes, a 2.3 L/D ratio, and a 60° entry angle was used for these experi-

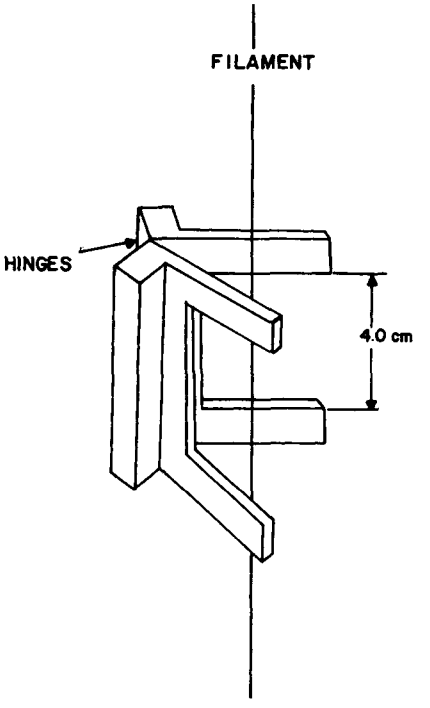

Fig. 1. Device for trapping linear density samples.

ments. Extrusion temperature was maintained at 290°C. The fibers emerged from the spinnerette into an atmosphere at 22°C. Cooling of the filaments was by free convection. The filaments were wound onto a godet and a take-up device with surface speeds of 420 cm/sec and 425 cm/sec, respectively.

Once the system was operating, threadline surface temperature measurements were made with a Hastings-Raydist Match-Temp Pyrometer (Model TM-2A) and Threadline Probe (TG-4). This null-balance pyrometer was used in conjunction with a 10-millivolt recorder. Threadline force at the first godet was measured with a Rothschild tensiometer equipped with a 0–4-gram head. Linear density samples of the threadline were taken with the device shown in Figure 1. The trapping procedure involved closing the trap on a single filament, simultaneously cutting the filament below the lower edge of the trap, followed by cutting the filament above the upper edge. This left an untouched 4-cm sample ready for subsequent subdivision, collation with other replicate samples, and weight measurement. The trapping arms of the device deformed the two ends of the sample filament so that indexing the distance from the spinnerette was simple. Mass throughput rate was determined from denier measurements of the filaments and knowledge of the take-up surface speed. Distance from the spinnerette to the first godet, x_L, was 442 cm.

RESULTS AND DISCUSSION

Threadline Surface Temperature

A typical profile of threadline surface temperature is shown in Figure 2 for polymer C. The general shape of the profile was observed to be the same for each polymer, and the profiles showed no discernable effect of molecular weight on the cooling behavior of the polymers. Approximately 5 to 6 cm from the spinnerette, the surface temperature of the filaments was found to be below the melting temperature T_m of the polymer (ca. 255°C) for all polymers. And at a distance $x = 40$ centimeters, the filament surface temperature was below the glass transition temperature T_g of the polymer. Careful use of the temperature pyrometer permitted measurement of temperatures as high as 30°C above T_m and at distances within 2 cm of the spinnerette. Thus, temperature measurements over essentially the entire threadline path were made. No attempt was made to determine the radial temperature profile.

Nonlinear least-squares fits of the temperature data to the functional relation

$$T_s(x) = a_1 e^{b_1 x} + c_1 \tag{8}$$

were successful, where $T_s(x)$ is threadline surface temperature (°C) at distance x, and a_1, b_1, and c_1 are constants. Experimental data are shown as the points. Values for a_1, b_1, and c_1 determined to be the "best fit"

TABLE II
Values of Coefficients of Eqs. (8) and (12)

	Eq. (8)—$T_s(x)$			Eq. (12)—$\rho A(x)$		
Polymer	a_1	$b_1 \times 10^2$	c_1	$a_2 \times 10^4$	$b_2 \times 10^1$	$c_2 \times 10^5$
A	275.4	−4.12	16.3	1.873	−3.657	1.671
B	304.2	−3.80	2.0	2.143	−4.040	1.546
C	284.2	−4.18	13.4	2.816	−4.548	1.530
D	290.8	−3.98	9.0	1.886	−4.083	1.409

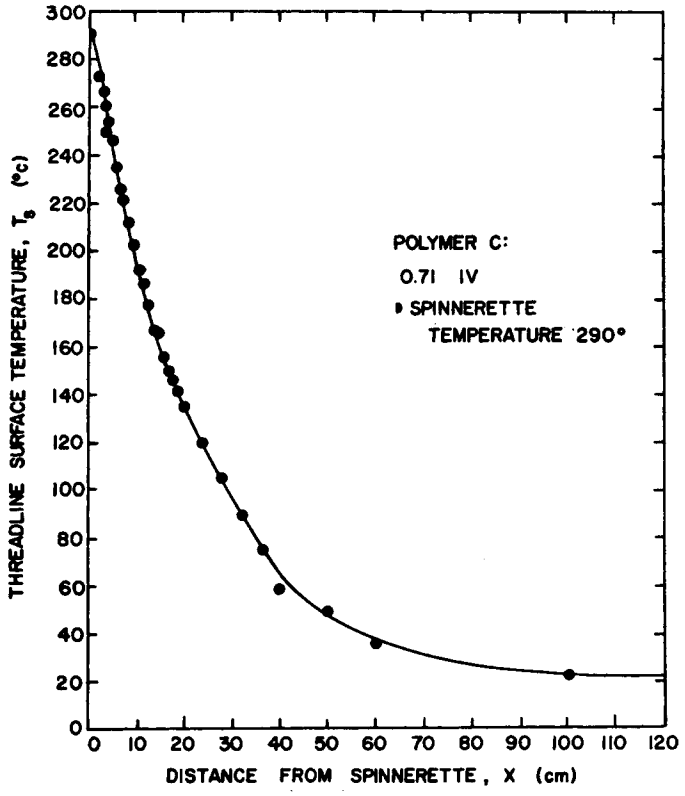

Fig. 2. Typical axial threadline surface temperature profile.

are given in Table II for the four polymers. Because of the relatively poor fit of eq. (8) in some regions and because of variation in some of the values for a_1, b_1, and c_1, the experimentally determined surface temperatures were used for subsequent calculations instead of the functional form of eq. (8). These data do, however, show behavior similar to that obtained by other workers.[4,5,24]

Threadline Density

It is apparent from eq. (7) that the density ρ is necessary for the determination of η_E. The approach taken in this study was to use the surface

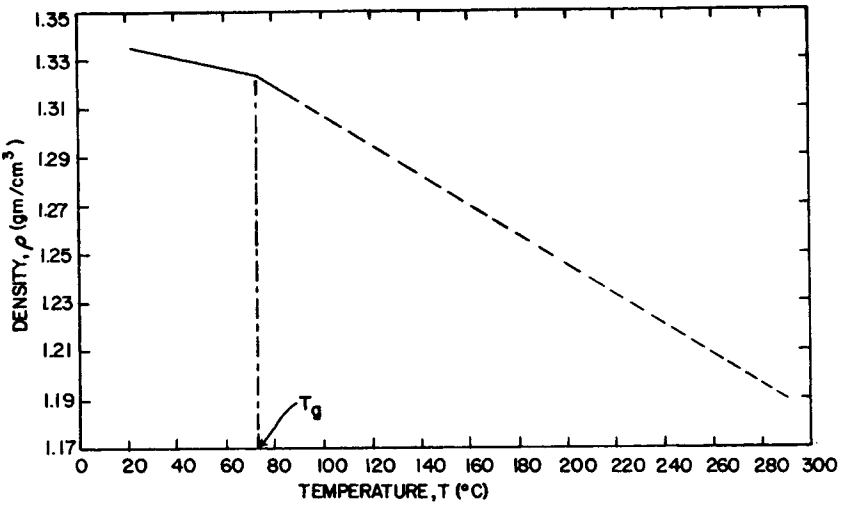

Fig. 3. Density–temperature relationship based on dilatometric study (solid line). Extrapolation to melt density (broken line).

temperature profiles, in conjunction with dilatometric data, to determine $\rho(x)$. This approach is taken as an approximation of $\rho(x)$ and as an improvement over the assumption of constant threadline density that is sometimes used.

Dilatometric data were obtained in these laboratories on these same polymers by Chao.[25] Figure 3 shows the variation of density with temperature.

Linear extrapolation between 95°C and 290°C was made to determine $\rho(T)$ between these temperatures. This assumes little or no crystallization has occurred, which is a reasonable assumption in spinning PET.

From Chao's data, the following expressions were used to obtain $\rho(T)$ for the four polymers:

$$V_{sp}(T) = 0.7274 + 3.857 \times 10^{-4}T \qquad (T \geqslant T_g) \tag{9}$$

$$V_{sp}(T) = 0.7461 + 1.303 \times 10^{-4}T \qquad (T < T_g) \tag{10}$$

$$\rho(T) = 1/V_{sp}(T). \tag{11}$$

The coefficients of the temperature term in eqs. (9) and (10) are average values of the slopes for the polymers above and below T_g, respectively.

Threadline Linear Density

A typical axial profile of linear density ρA is shown in Figure 4 for polymer C. Experimentally obtained ρA values are shown by the points. No molecular weight effect was apparent from the observed profiles.

The greatest material deformation occurs within the first 10 cm. At this distance, the linear density has reached essentially its final value (i.e., final denier). Samples between 3 and 33 cm from the spinnerette were

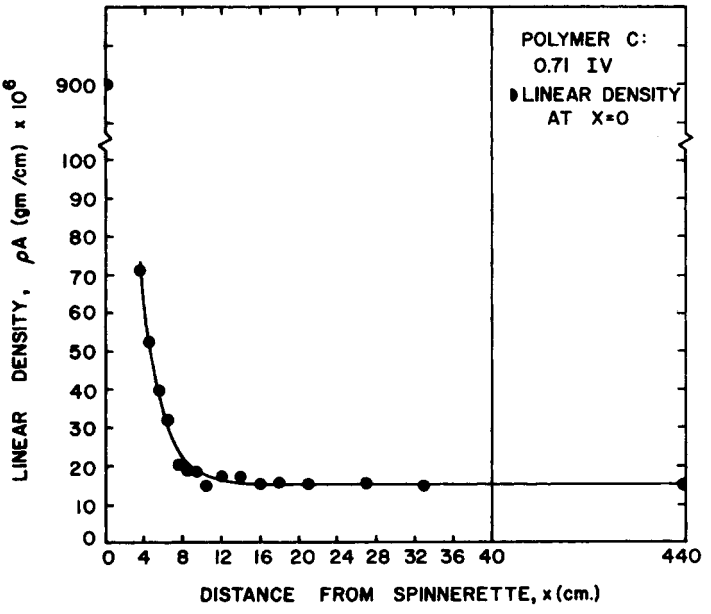

Fig. 4. Typical linear density profile: experimental data points (circles), "best fit" to eq. (12) (solid line).

taken. Collection of samples closer than 3 cm was not possible and those greater than 33 cm were unnecessary. The exact behavior within the first 3 cm is not known. It is apparent from Figure 4 that a tremendous change in ρA occurs during the first few centimeters.

Nonlinear least-squares fits of the linear density data to the functional relation

$$\rho A(x) = a_2 e^{b_2 x} + c_2 \qquad (3 \leqslant x \leqslant x_L) \tag{12}$$

were quite successful, where $\rho A(x)$ is linear density (g/cm) at distance x, and a_2, b_2, and c_2 are constants. The "best fit" of eq. (12) is shown by the solid line in Figure 4. The equation only applies, however, over the distance range of $x = 3$ to x_L cm. Values of a_2, b_2, and c_2 for the four polymers are given in Table II. Good agreement between observed data and values predicted by eq. (12) for the four polymers justified using the appropriate form of this equation for $\rho A(x)$. However, it must be pointed out that the coefficients a_2, b_2, and c_2 reflect the nature of their particular data. The importance of this will be pointed out in the discussion of elongation rate.

Since eq. (12) is a continuous function for $\rho A(x)$ over the range $3 \leqslant x \leqslant 442$ cm and is differentiable, $d(\rho A)/dx$ can be obtained directly. Thus, differentiating eq. (12) with respect to x gives

$$\frac{d(\rho A)}{dx} = a_2 b_2 e^{b_2 x} \qquad (3 \leqslant x \leqslant x_L). \tag{13}$$

This approach provides us with continuous functions for both ρA and $d(\rho A)/dx$ and eliminates the use of graphic techniques. It can be seen here that the values of the coefficients a_2 and, particularly, b_2 can strongly affect the results of subsequent calculations.

Threadline Velocity

In considering the threadline velocity, the radial velocity gradient was assumed to be zero. The velocity at any distance, $V(x)$, can be obtained from eq. (2), the continuity equation, that is,

$$\left.\begin{aligned} V(x) &= \frac{G}{\rho A(x)} && (14) \\ &= \frac{G}{a_2 e^{b_2 x} + c_2} && (15) \end{aligned}\right\} \quad (3 \leqslant x \leqslant x_L).$$

Data for G, the mass throughput rate are given in Table III for the four polymers.

A typical velocity profile (for polymer C) is shown in Figure 5. In all polymers, an inflection was observed at approximately 6 cm. Ziabicki and Kedzierska[1] have suggested that the inflection in the velocity profile was an effect of a structural transition occurring in the threadline; and in the case of melts, the transition was probably one of solidification. The position of the inflection in this study is several centimeters below the position at which the filament surface temperature reaches T_m of the polymer.

The general shape of the velocity profiles is the same for each of the four polymers. The break in the solid line in Figure 5 is due to the lack of data in that region. The exact behavior in this region is not known since no quantitative measures of die swell were made. The degree of die swell was, however, observed to be small at these throughput rates. Note that the velocity increases rapidly over the first 20 cm and then levels off to the first godet velocity V_1.

Average velocity at the spinnerette exit, $V(0)$, was calculated using the spinnerette hole area, the mass throughput rate, and the melt density of the polymer. The results of this calculation for the four polymers are also given in Table III. Also given in Table III are values from

TABLE III
Mass Throughput Rates, Exit Velocity, and Shear Rate at the Wall for the Polymers Studied

Polymer	G g/min	G (g/sec/hole) $\times 10^3$	$V(0)$, cm/sec	$\dot{\gamma}_w$, $\sec^{-1}$
A	2.911	6.93	7.70	1990
B	2.836	6.79	7.55	1940
C	2.631	6.26	6.96	1800
D	2.540	6.05	6.72	1740

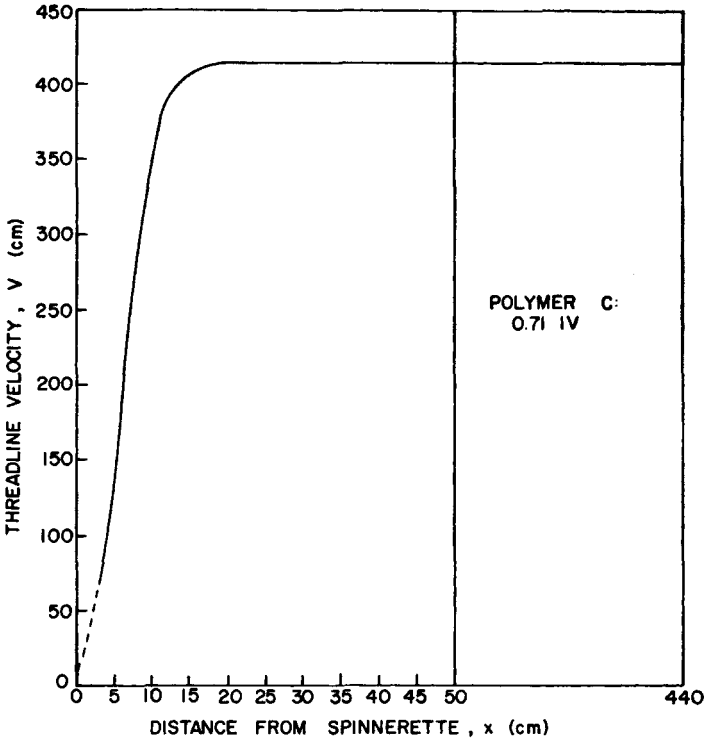

Fig. 5. Typical threadline velocity profile: $V(0) = 6.96$ cm/sec.

the shear rate at the capillary wall, $\dot{\gamma}_w$. These values are based on the assumption of Newtonian flow, i.e.,

$$\dot{\gamma}_w = \frac{4Q}{\pi R^3} \tag{16}$$

where Q is volumetric throughput rate ($Q = G/\rho$) and R is the capillary radius. These values are given for informational purposes only.

Threadline Elongation Rate

The importance of elongation rate $\dot{\gamma}_E$ to the elongational viscosity has been emphasized in the literature. Although eq. (7) does not involve $\dot{\gamma}_E$ explicitly, it is an implicit component as pointed out earlier. The elongation rate expressed in terms of the parameters ρA and G is given by

$$\dot{\gamma}_E = \frac{-G}{(\rho A)^2} \frac{d(\rho A)}{dx} \tag{17}$$

$$= \frac{-Ga_2b_2e^{b_2x}}{(a_2e^{b_2x} + c_2)^2}. \tag{18}$$

At this point, it is evident that the numerical value obtained for elongation rate is strongly dependent on the values of the coefficients a_2, b_2, and

TABLE IV
Maximum Values of $\dot{\gamma}_E$ and Distance at Which the Maximum Values Occur

Polymer	$\dot{\gamma}_{E,\max}$, $\sec^{-1}$	x^*, cm
A	37.9	6.6
B	44.1	6.5
C	47.2	6.4
D	43.8	6.4

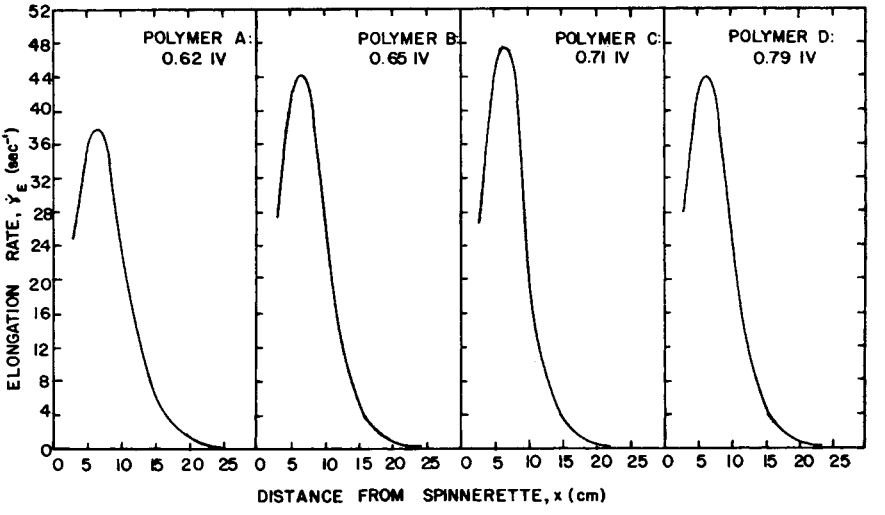

Fig. 6. Threadline elongation rate profiles for the four polymers studied.

c_2, which may change slightly depending on the data. Figure 6 shows the results of calculations using eq. (18).

The most evident feature of these elongation rate profiles is the maximal point. The maximal point obviously corresponds to the inflection point of the velocity profiles. By setting the derivative of $\dot{\gamma}_E$ with respect to x equal to zero, i.e., $d\dot{\gamma}_E/dx = 0$, it is possible to derive a relation to obtain the distance at which the maximal point occurs, x^*. This relation is given by

$$x^* = \frac{-\ln (a_2/c_2)}{b_2}. \tag{19}$$

Similarly, the maximum value of the elongation rate $\dot{\gamma}_{E,\max}$ for each polymer can be obtained from the following relation:

$$\dot{\gamma}_{E,\max} = \frac{-V(x)}{\rho A(x)} \frac{d(\rho A(x))}{dx}\bigg|_{x=x^*}. \tag{20}$$

The results of computations using eqs. (19) and (20) are shown in Table IV. Notice that x^* appears to be the same for each of the four molecular weights. This implies that the elongation rate reaches its maximum value at the

same distance from the spinnerette for each of the four polymers. Comparing these distances with the temperature profiles indicates that $\dot{\gamma}_{E,\max}$ occurs at threadline surface temperatures between 225° and 240°C. The apparent increase and then decrease of $\dot{\gamma}_{E,\max}$ is considered to be only a reflection of the behavior of the coefficients a_2, b_2, and c_2, and it is felt that no conclusions regarding this behavior can be made at this time due to the limited data.

After reaching a maximum, the elongation rate decreases rapidly to zero at distance of 40 cm. This corresponds to the region of constant velocity in the velocity profiles. At this point, the filaments have reached their final denier.

Threadline Force Components

Theoretical analysis of the components of force acting on a moving melt-spun threadline has been widely discussed in the literature.[3-6,14,16,18] An equation of force balance, as suggested by Ziabicki,[3,6] can be written as

$$F_{\text{rheo}}(x) = F_{\text{ext}} + F_{\text{grav}}(x) + F_{\text{aero}}(x) + F_{\text{inert}}(x) + F_{\text{surf}}(x). \quad (21)$$

The components of the force balance are: $F_{\text{rheo}}(x)$, rheological force; F_{ext}, external force; $F_{\text{grav}}(x)$, gravitational force; $F_{\text{aero}}(x)$, aerodynamic drag force; $F_{\text{inert}}(x)$, intertial force; and $F_{\text{surf}}(x)$, force from surface tension.

The rheological force is the force imparted by the material's resistance to flow deformation and is the component of primary interest in any elongational flow study. Forces acting in the same direction as the filament velocity are taken as positive. The experimentally obtained external force per filament, F_{ext}, is shown in Figure 7 for the four polymers. A linear relationship exists over this intrinsic viscosity range. This relationship is given by

$$F_{\text{ext}} = -399.7 + 812.8[\eta]. \quad (22)$$

The gravitational force component $F_{\text{grav}}(x)$ is due to the weight of the hanging filament. $F_{\text{grav}}(x)$ was calculated from the relation

$$F_{\text{grav}}(x) = \int_x^{x_L} g\rho A(x) \qquad (3 \leqslant x \leqslant x_L) \quad (23)$$

where g is the acceleration of gravity.

The force component due to air drag was computed from a relation based on Sakiadis' treatment[26] of a continuous cylinder running in a stationary medium. This relation is

$$F_{\text{aero}}(x) = -0.843(\rho^0/\rho(x)GV(x))[\pi\rho(x)\nu^0(x_L - x)/G]^{0.915} \quad (24)$$

where ρ^0 is the density of the surrounding air and ν^0 is the kinematic viscosity of the air. This same treatment has been used by several workers.[6,14,18]

The force required to accelerate the filament from $V(0)$ to its final velocity V_L is given by

$$F_{\text{inert}}(x) = -G[V_L - V(x)]. \quad (25)$$

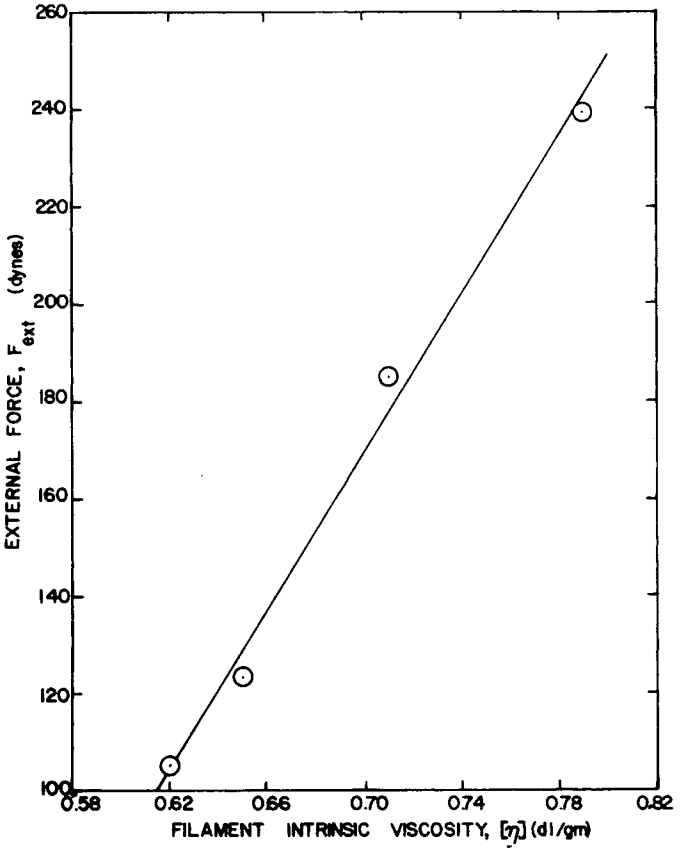

Fig. 7. External force per filament vs. filament intrinsic viscosity. Experimental data points (circles). Least-squares fit to a straight line (solid line).

The surface tension component of force $F_{surf}(x)$ has been neglected in this study. Previous studies[3,4,14,18] have also neglected this component.

The distribution of force components for a typical polymer (C) is shown in Figure 8. Similar behavior was observed for the remaining polymers. $F_{inert}(x)$ is essentially zero except within the first few centimeters where acceleration is occurring. $F_{grav}(x)$ and $F_{aero}(x)$ are about equal in magnitude but opposite in direction, thus tending to offset each other. Thus, $F_{rheo}(x)$ and F_{ext} are about equal, so that for these spinning conditions the other force components could have been neglected.

Profiles of $F_{rheo}(x)$ for the four polymers are shown in Figure 9 for purposes of comparison. Again, $F_{rheo}(x)$ increases linearly with intrinsic viscosity.

Axial tensile stress σ_{xx} was computed from the relation

$$\sigma_{xx} = \frac{F_{rheo}(x)\rho(x)}{\rho A(x)}. \tag{26}$$

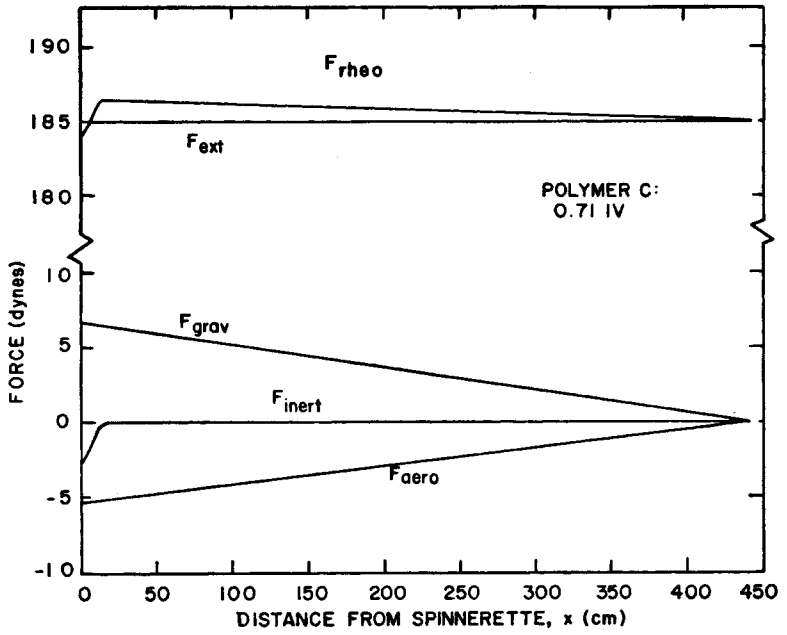

Fig. 8. Axial distribution of threadline force components per filament.

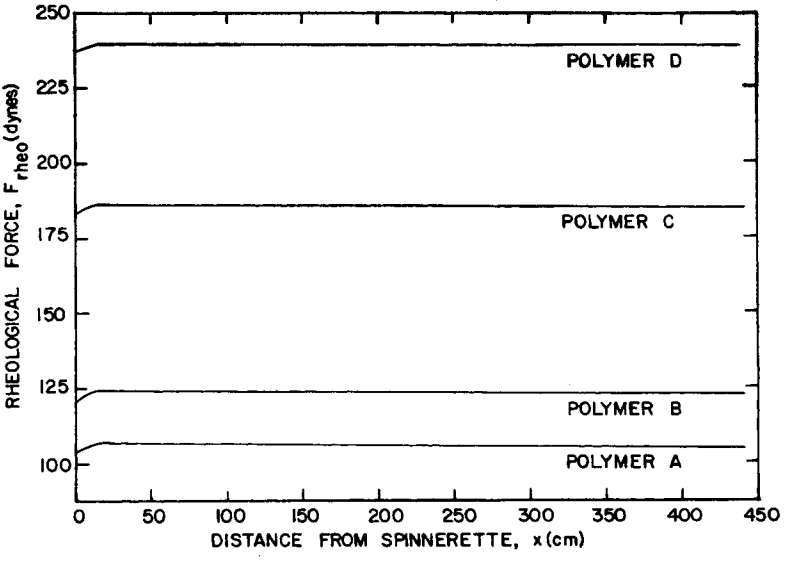

Fig. 9. Rheological force per filament as a function of axial distance from the spinnerette for the polymers studied.

Axial stress profiles are shown in Figure 10 for the four polymers. These profiles are very similar in shape to those reported by Ziabicki.[3]

Elongational Viscosity

Elongational viscosity was calculated from eq. (7) using the relations for the parameters presented here. The results of these calculations plotted

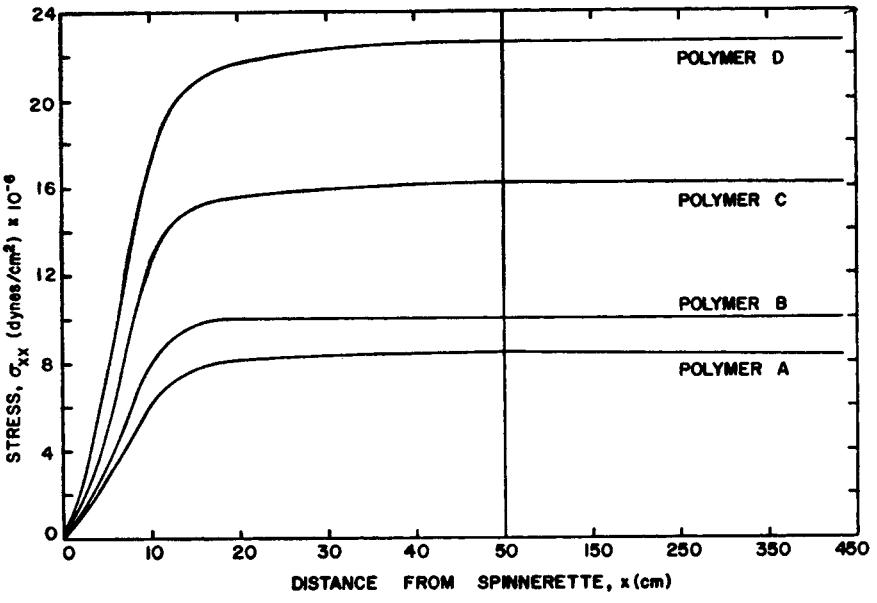

Fig. 10. Axial tensile stress per filament as a function of distance from the spinnerette for the polymers studied.

versus distance from the spinnerette are shown in Figure 11 for polymer C. This plot is made only to show that elongational viscosity increases exponentially with distance along the spinning path. However, η_E does not explicitly depend on distance, but depends on temperature and elongation rate. The profile shown in Figure 11 does not consider these parameters, but merely indicates the dramatic change that occurs with distance due to the changes occurring in $\dot{\gamma}_E$ and T.

The increase in elongational viscosity is due to both a strong temperature effect and an elongation rate effect. The change in these parameters result in an increase in the resistance to flow deformation, and hence η_E increases. However, in nonisothermal spinning such as in this study, the increase in η_E is readily observed, but the contributions of temperature and elongation rate are not readily apparent. Only when one parameter is maintained constant, such as in isothermal spinning, can the effect of the remaining parameter be quantitatively measured. No isothermal studies on PET which consider the effect of $\dot{\gamma}_E$ on η_E have appeared in the literature.

Arrhenius plots such as shown on Figure 12 can be useful if used properly. These plots show η_E plotted versus an inverse function of absolute temperature for the four polymers. One must be careful, however, to remember that since both $\dot{\gamma}_E$ and T are changing along the spinning path, the data shown in this figure still contain a contribution of elongation rate. The three-dimensional nature of the relationship between η_E and $\dot{\gamma}_E$ and T make data presentation difficult. However, a look at Figure 12 indicates that since the elongation rates are about the same for each polymer, at a specified temperature, qualitatively the elongational viscosity increases with molecular weight. As shown in Figure 6, the elongation rates are

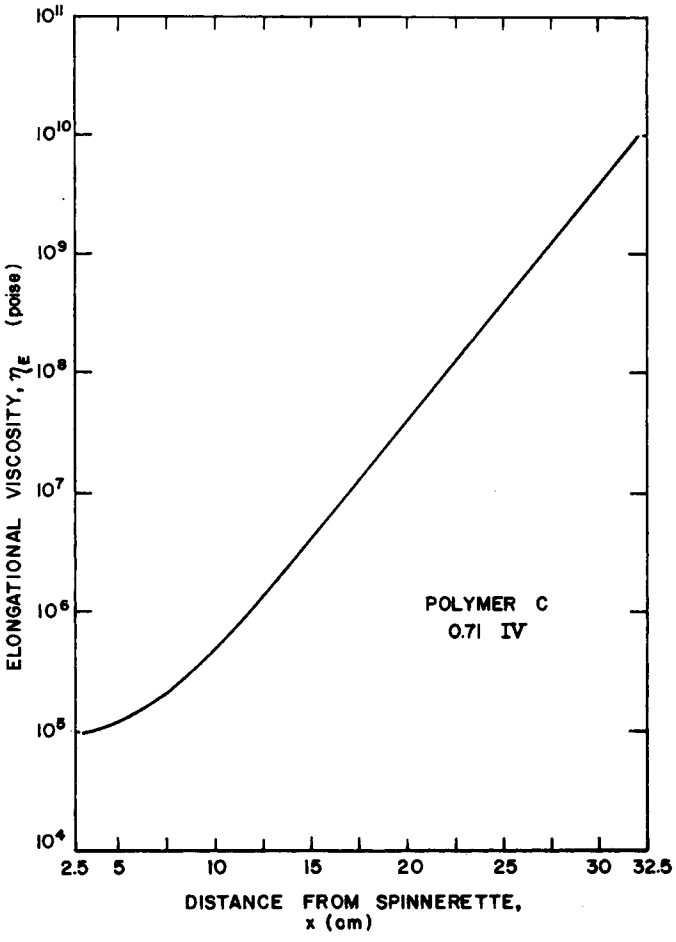

Fig. 11. Typical semilogarithmic plot of elongational viscosity vs. distance from the spinnerette.

about the same, except in the region where $x = 5$ to 10 cm (ca. 250° to 200°C). Comparing η_E for the four polymers at temperatures in the region where elongation rates are the same clearly indicates an increase in η_E with molecular weight. Even in the region (5 to 10 cm, or 250° to 200°C) where the elongation rates give the appearance of differing most, the same behavior is observed, indicating possibly a mild effect of $\dot{\gamma}_E$ on η_E. However, the significance of any apparent difference in elongation rates between polymers in this region is not known at present. The crossing of the profile for polymers B and C is not considered to be significant.

Activation Energy

Kase and Matsuo[4] and others[14] have used Arrhenius plots to obtain an activation energy of elongational flow E_a^e. They have, however, assumed

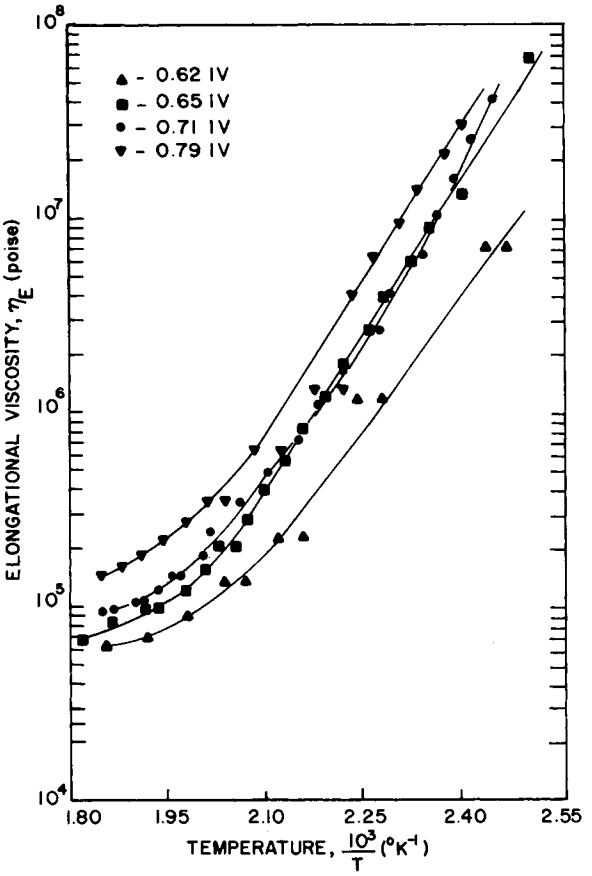

Fig. 12. Semilogarithmic plot of elongational viscosity vs. inverse absolute temperature for the polymers studied.

that the elongation rate was negligible and that η_E depended only on temperature (i.e., exhibited Newtonian behavior). This assumption was not made here. Instead, an attempt was made to obtain an activation energy that is assumed to depend explicitly on elongation rate. In shear flow it has been shown by Bernhardt[27] and Combs et al.[28] that activation energy of shear flow, E_a^s, is a decreasing function of shear rate at constant temperature for certain polymers.

To obtain an expression for E_a^e $(\dot{\gamma}_E)$, activation energy of elongational flow, as a function of $\dot{\gamma}_E$, an attempt was first made to fit the elongational viscosity, elongation rate, and absolute temperature data to a polynomial. Only data in the rubbery and liquid regions $(>T_g)$ were used in this fit. The two independent parameters of this polynomial are $\dot{\gamma}_E(x)$ and $10^3/T(x)$, and the polynomial has the form

$$\log_{10}\eta_E(x) = \alpha_0 + \alpha_1\left(\frac{10^3}{T}\right) + \alpha_2(\dot{\gamma}_E) + \alpha_3\left(\frac{10^3}{T}\cdot\dot{\gamma}_E\right) \qquad (27)$$

TABLE V
Values of Coefficients of Eq. (27)

Polymer	α_0	α_1	α_2	α_3
A	−5.03	4.95	0.207	−0.101
B	−4.38	4.86	0.146	−0.075
C	−6.41	5.77	0.187	−0.091
D	−4.08	4.83	0.166	−0.085

where α_i are constants for $i = 0, 1, 2$, and 3. Nonlinear least-squares fits of the data to this polynomial were good. The values for the coefficients α_0, α_1, α_2, and α_3 are given in Table V.

Activation energy E_a^e was obtained by differentiating eq. (27) with respect to $10^3/T$ and multiplying this slope by the conversion factor of (2.303) (10^3) (R)kcal/mole. Thus, E_a^e is given by

$$E_a^e = \frac{d(\log_{10}\eta_E)}{d\left(\frac{10^3}{T}\right)} (2.303)(0.001987)(10^3) \tag{28}$$

$$= 4.576(\alpha_1 + \alpha_3\dot{\gamma}_E). \tag{29}$$

The relationships obtained for the four polymers are given in Table VI. Note that E_a^e for all polymers is a decreasing function of $\dot{\gamma}_E$. At zero elongation rate ($\dot{\gamma}_E = 0$), E_a^e is about 22 to 26 kcal/mole. These values are in very good agreement with values obtained by Griswold[29] for zero shear rate activation energy of these same polymers. Also note that the relationships for E_a^e are consistent for the polymers. No effect of molecular weight on E_a^e is apparent within this $\bar{M}_w$ range.

The coefficients of eq. (27) and, hence, of eq. (29) were found to change slightly when data corresponding to lower temperatures were removed from the fits. However, the results presented here are considered to be acceptable as a first approximation of $E_a^e(\dot{\gamma}_E)$.

SUMMARY

A study of the threadline dynamics of poly(ethylene terephthalate) of four molecular weights has been presented. No effect of molecular weight on the temperature profiles of these polymers was observed. Nonlinear least-squares fits to the linear density data were quite good, thus permitting

TABLE VI
Relationships for E_a^e for the Polymers Studied

Polymer	Relationship for E_a^e, kcal/mole
A	$22.7 - 0.463\dot{\gamma}_E$
B	$22.2 - 0.342\dot{\gamma}_E$
C	$26.4 - 0.418\dot{\gamma}_E$
D	$22.1 - 0.388\dot{\gamma}_E$

use of an equation for both velocity and elongation rate profiles. The inflection point of the velocity profile, which corresponds to the maximum in the elongation rate profile, was found to occur at the same distance from the spinnerette and approximately the same temperature for each of the four polymers.

Comparison of the elongational viscosity for the four polymers over the entire temperature (and also elongation rate) range clearly indicated an increase in elongational viscosity with increasing molecular weight.

Good agreement was obtained in fitting the observed data to a polynomial relating elongational viscosity to the parameters elongation rate and temperature. Use of the polynomial also permitted first approximations of the activation energy of elongational flow E_a^e to be made. The activation energy was found to be a decreasing linear function of elongation rate for all polymers. Slight variation in E_a^e were found to exist for the four polymers when evaluated at zero elongation rate. These zero elongation rate activation energies are in good agreement with zero shear rate activation energies of these same polymers.

Further study is needed to determine the effect of elongation rate on the elongational viscosity of PET. The dependence of activation energy of elongational flow on elongation rate also needs further investigation. These are the objectives of our current research.

The authors are grateful to the Goodyear Tire and Rubber Company for both financial assistance and for supplying the polymers used in this study. We also wish to thank N.P.C. Chao for the dilatometric data, and P. D. Griswold and A. S. Abhiraman for their technical assistance and helpful discussions. Appreciation is also extended to Dr. R. J. Hader for help with the statistical interpretation.

References

1. A. Ziabicki and K. Kedzierska, *Kolloid Z.*, **171**, 51 (1960).
2. A. Ziabicki and K. Kedzierska, *Kolloid Z.*, **171**, 111 (1960).
3. A. Ziabicki, *Kolloid Z.*, **175**, 14 (1961).
4. S. Kase and T. Matsuo, *J. Polym. Sci. A*, **3**, 2541 (1965).
5. S. Kase and T. Matsuo, *J. Appl. Polym. Sci.*, **11**, 251 (1967).
6. A. Ziabicki, in *Man-Made Fibers: Science and Technology*, Vol. 1, H. F. Mark, S. M. Atlas, and E. Cernia, Eds. Wiley, New York, 1967.
7. C. D. Han, *Rheol. Acta*, **9**, 355 (1970).
8. R. L. Ballman, *Rheol. Acta*, **4**, 137 (1965).
9. F. N. Cogswell, *Rheol. Acta*, **8**, 187 (1969).
10. I. Hamana, *Melliand Textilber.*, **50**, 499 (1969).
11. Y. Ohzawa, Y. Nagano, and T. Matsuo, *J. Appl. Polym. Sci.*, **13**, 257 (1969).
12. C. D. Han and L. Segal, *J. Appl. Polym. Sci.*, **14**, 2973 (1970).
13. C. D. Han and L. Segal, *J. Appl. Polym. Sci.*, **14**, 2999 (1970).
14. T. Ishibashi, K. Aoki, and T. Ishii, *J. Appl. Polym. Sci.*, **14** 1597 (1970).
15. Y. Ohzawa and Y. Nagano, *J. Appl. Polym. Sci.*, **14**, 1897 (1970).
16. D. Acierno, J. N. Dalton, J. M. Rodriquez, and J. L. White, *J. Appl. Polym. Sci.*, **15**, 2395 (1971).
17. F. N. Cogswell, *Trans. Soc. Rheol.*, **16**, 383 (1972).
18. C. D. Han and R. R. Lamonte, *Trans. Soc. Rheol.*, **16**, 447 (1972).
19. R. R. Lamonte and C. D. Han, *J. Appl. Polym. Sci.*, **16**, 3285 (1972).

20. J. Meissner, *Trans. Soc. Rheol.*, **16**, 405 (1972).
21. F. T. Trouton, *Proc. Roy. Soc.*, **A77**, 426 (1906).
22. H. Nitschmann and J. Schrade, *Helv. Chem. Acta*, **31**, 297 (1948).
23. M. L. Wallach, *Makromol. Chem.*, **103**, 19 (1967).
24. E. H. Andrews, *Brit. J. Appl. Phys.*, **10**, 39 (1959).
25. N. P. C. Chao, unpublished report, 1973.
26. B. C. Sakiadis, *A.I.Ch.E.J.*, **7**, 467 (1961).
27. E. C. Bernhardt, *Processing of Thermoplastic Materials*, Reinhold, New York, 1969, p. 40.
28. R. L. Combs, D. F. Slonaker, and H. W. Coover, Jr., *Tech. Papers, SPE Meeting*, Detroit, Mich., May, 1967.
29. P. D. Griswold, unpublished report, 1973.

Received December 5, 1973
Revised February 13, 1974